JMEPEG (2011) 20:1600–1605
DOI: 10.1007/s11665-011-9835-1

1059-9495/$19.00

Tribocorrosion Behavior of Aluminum/Alumina Composite Manufactured by Anodizing and ARB Processes

Roohollah Jamaati, Mohammad Reza Toroghinejad, Jerzy A. Szpunar, and Duanjie Li

(Submitted September 19, 2010; in revised form December 7, 2010)

In the present work, tribocorrosion behavior of Al/Al_2O_3 composite strips manufactured by anodizing and accumulative roll bonding (ARB) processes was investigated. The alumina quantity was 0.48, 1.13, and 3.55 vol.% in the aluminum matrix. Tribocorrosion experiments were conducted using a ball-on-plate tribometer, where the sliding contact was fully immersed in 1 wt.% NaCl solution. The composite sample served as a working electrode and its open circuit potential (OCP) was monitored before, during, and after sliding. In order to characterize the electrochemical behavior of the surface before and after sliding electrochemical impedance spectroscopy (EIS) was used and wear was also measured. Furthermore, the influence of quantity and distribution of reinforcement particles in the matrix on OCP and EIS was evaluated. It was found that the quantity, shape, size, and dispersion of alumina particles in the aluminum matrix strongly affected the measured tribocorrosion characteristics. The results showed that inhomogeneous, lower quantity, fine, and acicular-shape alumina particles cause serious materials loss in tribocorrosion process.

Keywords joining, metal-matrix composites, optical microscopy, rolling, tribology

1. Introduction

Tribocorrosion or corrosion-wear describes the material behavior in systems where interactions between wear and corrosion processes take place. In such a tribocorrosion system, materials are subjected to mechanical, chemical, and electrochemical loadings (Ref 1). Examples include degradation of articulation prosthesis and dental fillers, accelerated corrosion of steel conveyors exposed to ambient air of high humidity, erosion-corrosion of slurry pipes, and numerous others (Ref 1, 2). Passive metals are particularly sensitive to tribocorrosion because rubbing can destroy their passive surface film that may enhance both corrosion and wear rate before the surface repassivates. It has been observed that the material removal during tribocorrosion process usually exceeds the sum of mechanical and corrosion contributions measured separately (Ref 1). Thus, understanding the behavior of passive metals under tribocorrosion conditions is of great scientific interest and also very important for their applications.

Lightweight, high-strength metallic alloys are attractive for the applications in transportation industries since reduction in weight results in improved fuel economy. The main drawback with most lightweight alloys is a relatively low-elastic modulus (Ref 3). Aluminum metal-matrix composites (Al MMCs) are being considered as a group of new advanced materials for their light weight, high strength, high-specific modulus, low coefficient of thermal expansion and good wear resistance properties. Combination of these properties is not available in most of the conventional materials. Recently, Al matrix composites have been used in various automobile products (Ref 4).

Processing techniques for Al MMCs can be classified into (a) powder metallurgy (Ref 5, 6), (b) liquid state processing (Ref 7, 8), and (c) solid state processing (Ref 9-13). The present authors (Ref 11, 12) developed the accumulative roll bonding (ARB) process as a new solid state technique for the manufacture of aluminum/alumina composite. This ARB process can be used for making high strength and highly uniform MMCs.

Over the past years, a number of authors have investigated the tribocorrosion behavior of composites. Bratu et al. (Ref 14) studied the tribocorrosion behavior of Ni-SiC composite coatings under lubricating conditions. Also, Benea et al. (Ref 1) evaluated the tribocorrosion behavior of Ni-SiC nanostructured composite coatings obtained by electrodeposition. The literature data about tribocorrosion behavior of MMCs is, however, very limited.

The aim of this study is to investigate the effect of size and quantity of alumina particles dispersion in the aluminum matrix on the tribocorrosion behavior of Al/Al_2O_3 composite produced by anodizing and ARB processes in an aqueous corrosion environment.

2. Experimental Procedure

The materials used in this study were fully annealed strips of commercial purity aluminum alloy [specifications are given in

Roohollah Jamaati and **Mohammad Reza Toroghinejad**, Department of Materials Engineering , Isfahan University of Technology, Isfahan 84156-83111, Iran; **Jerzy A. Szpunar**, Department of Mechanical Engineering, University of Saskatchewan, Saskatoon, SK S7N 5A9, Canada; and **Duanjie Li**, Department of Materials Engineering, McGill University, Montreal, QC H3A 2B2, Canada. Contact e-mail: r.jamaatikenari@ma.iut.ac.ir.

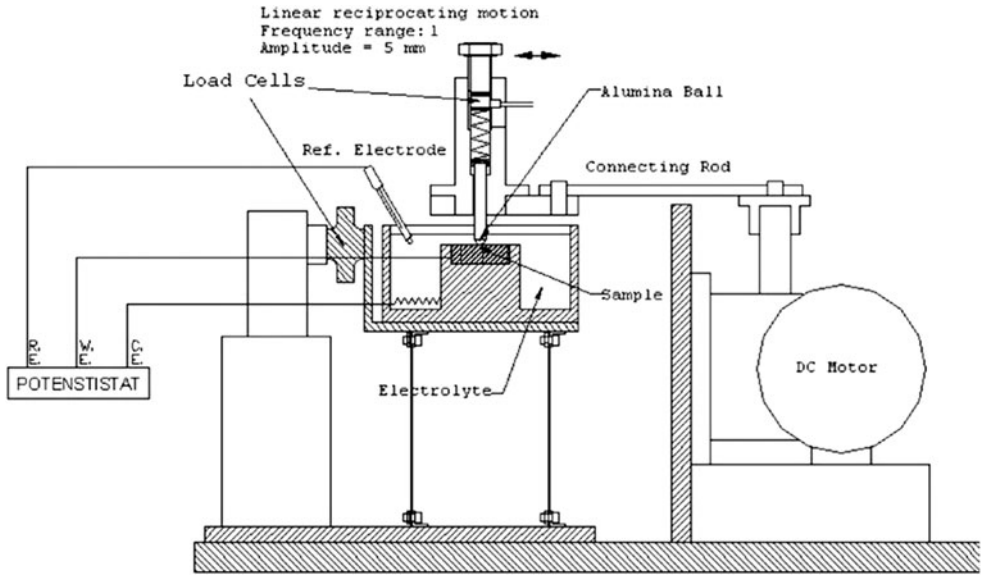

Fig. 1 The schematic illustration of tribocorrosion apparatus (Ref 2, 21)

our previous article (Ref 12)]. The dimension of all the strips was 200 mm in length, 50 mm in width, and 0.4 mm in height. Some of the strips were anodized in 15 wt.% sulfuric acid under an applied voltage of 16 V for three different times (1, 5, and 60 min) in order to produce three different oxide film thicknesses. Prior to anodizing, the samples were cleaned in NaOH and then in an HNO_3 bath. Chemical compositions of the baths are given in our previous paper (Ref 12). To ensure a constant and homogeneous temperature throughout the solution, forced convection was provided by electrolyte stirring. The oxide layers were formed at a low-electrolyte temperature (16 °C) that favors rapid oxide growth and the reduction of dissolution of the oxide layer. Then, strips were neutralized in ammonium acetate (Ref 12) under an applied voltage of 16 V for 15 min to enhance bonding in the ARB process. The thickness of the alumina layers obtained during anodizing was determined by scanning electron microscopy observation of the oxide cross sections. Average values of thickness and standard deviations for about 20 measurements were calculated. The alumina coating thicknesses on anodized Al 1100 for 1, 5, and 60 min were 2.2 ± 0.1, 5.1 ± 0.2, and 16 ± 0.5 μm, respectively. In this study, the ARB process included two steps. In the first step, the two strips (nonanodized) were degreased in acetone bath and scratch brushed with a stainless steel brush wire 0.26 mm in diameter. Then, the anodized strip was laid between the prepared surfaces of unanodized strips. The strips were stacked over each other, and then were fastened at both ends and roll-bonded in room temperature to 60% reduction. The roll-bonded strips were then cut in half. The aim of the second step was designing a uniform distribution of reinforcement particles in the matrix. In this step, the procedure described for the first step was repeated up to eight times with a reduction equal to 50% in each cycle. The schematic of the ARB process for manufacturing of the composite is illustrated in our previous work (Ref 12).

Tribocorrosion was measured on an area of 25 × 15 mm of the samples and at the subsurface region, 0.1 mm under the surface of the samples. These samples were prepared by the standard metallographic procedures (grinding and mechanical polishing). Tribocorrosion tests were performed using a linear reciprocating ball-on-plate tribometer. Figure 1 illustrates a schematic of the apparatus used. During the test, a 4.75-mm diameter alumina ball rubs on the sample surface immersed in the 1 wt.% NaCl solution. The reciprocating motion of the ball is realized by the classic slider-crank mechanism. The details of the experimental setup have been described previously (Ref 15). The sample served as the working electrode and its potential was controlled using Autolab PGSTAT302 potentiostat equipped with a frequency response analyzer. The counter electrode was made of coiled platinum wire, and the standard calomel electrode SCE (+241 mV vs. standard hydrogen electrode) was used as a reference for the potential measurements. The electrochemical impedance spectroscopy (EIS) measurements were performed before the sliding tests at the open circuit potential (OCP), using voltage amplitude of 10 mV in the frequency range of 100 kHz to 10 MHz. Afterward, the sliding started with normal load of 5 N. The stoke length was 5 mm and the number of wear cycles was 1800 at a frequency of 1 Hz.

The sequence of operations during the wear-corrosion experiment is schematically illustrated in Fig. 2. The tribocorrosion test consisted of the following steps: (a) in order to reach a stable potential during OCP measurement, the sample was immersed in Ringer's solution for 1 h (first region), (b) for characterizing the electrochemical behavior of the surface before rubbing, the EIS before the sliding wear test at the corrosion potential was measured (second region), (c) the OCP's values during and after the sliding wear test were monitored continuously (the third and fourth region), and (d) finally, in order to characterize the electrochemical behavior of the surface after sliding wear, and after wear test, the EIS at the corrosion potential was measured (the fifth region).

Nikon EPIPHOT 300 Optical microscope (OM) was used for microstructural observation before tribocorrosion experiment to find out how well the alumina particles were distributed in the produced composites after eight ARB cycles. Also, OM provided macroscopic images of wear areas after tribocorrosion test.

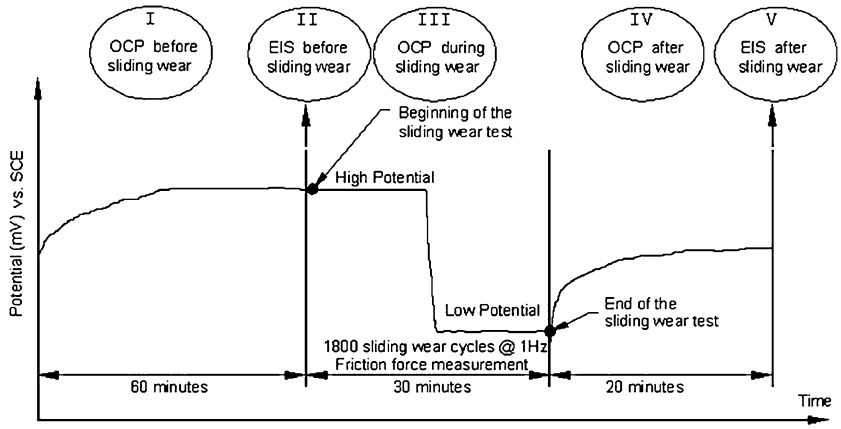

Fig. 2 Sequence of operations during the tribocorrosion experiment shown by the OCP evolution (Ref 2)

3. Results and Discussion

3.1 Microstructural Evolution of As-ARBed Samples

Microstructure of aluminum/alumina MMCs with various Al_2O_3 quantities (0.48, 1.13, and 3.55 vol.%) produced by eight ARB cycles at rolling direction-transverse direction (RD-TD) is presented in Fig. 3. All the samples exhibited a uniform distribution of alumina particles in aluminum matrix without any porosity and debonding. The size of alumina particles for MMCs with 0.48, 1.13, and 3.55 vol.% was about 1, 4, and 9 μm, respectively. It is important and interesting that the shape of alumina particles in Fig. 3(a) and (b) is spheroid, while for Al/3.55 vol.% Al_2O_3 composite strip the shape is angular and acicular. Also, for the composite with 3.55 vol.% alumina, a few clusters of particles were observed. The particles in these clusters were separated and fragmented but the distance between them is still low. However, all three composites showed a good homogeneity and strong interfacial bonding. This high-quality bonding is related to rolling pressure in each cycle and the porous nature of the alumina layer morphology produced by the anodizing process which is very important and helps a better bonding to occur (Ref 12).

3.2 OCP Measurements

Figure 4 demonstrates the results obtained from tribocorrosion experiments at OCP during and after sliding for the composites with 0.48, 1.13, and 3.55 vol.% reinforcement particles. From this figure, it is obvious that when rubbing starts at 150 s, the OCP of all the three samples undergoes a significant negative shift. The value of this shift is almost constant for all three composite strips. The drop in the potential is due to the depassivation process of aluminum matrix. It can be concluded that the shape and quantity of alumina particles do not have any effect on depassivation process of matrix. A protective oxide layer, namely alumina is formed due to the presence of electrolyte in contact with the aluminum surface. During the wear test, the oxide film is removed and the surface becomes active (depassivation process) and so, the surface is subjected to corrosion. Under these conditions, AA1100 aluminum undergoes anodic dissolution followed by the formation of a passive oxide film on the surface according to the following reactions (Ref 2, 16):

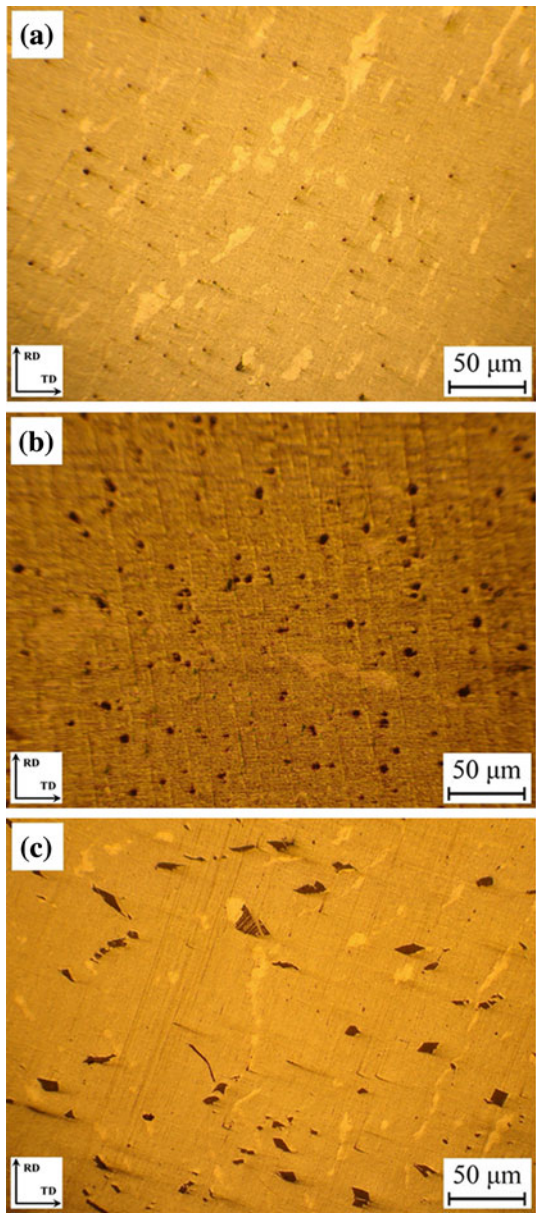

Fig. 3 OM images of the aluminum/alumina composites with (a) 0.48, (b) 1.13, and (c) 3.55 vol.% reinforcement produced by ARB process before testing

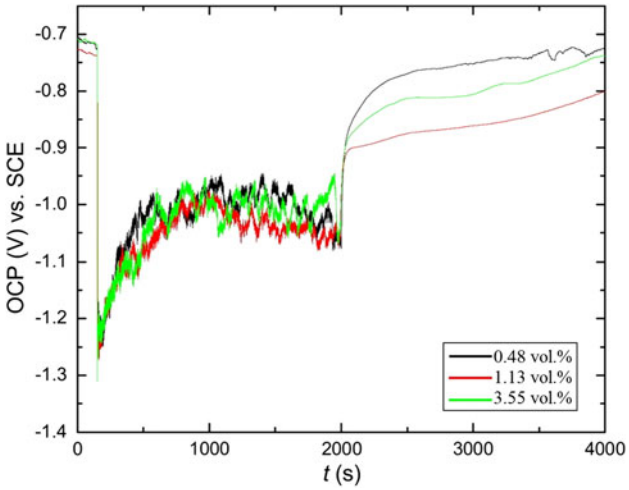

Fig. 4 OCP measurements during and after sliding test for ARBed samples with 0.48, 1.13, and 3.55 vol.% alumina

$$M \rightarrow M^{n+} + ne^{-} \quad \text{(Eq 1)}$$

$$mM + nH_2O \rightarrow M_mO_n + H^{+} + xe^{-}, \quad \text{(Eq 2)}$$

where M designates the metallic materials, in our case, mainly aluminum. The oxidation reactions (whether dissolution or oxide formation) take place in the wear track and generate electrons which must be consumed by the cathodic reaction in order for the oxidation reactions to proceed. Under these conditions, the main cathodic reaction supporting the passivation reaction is the reduction of the dissolved oxygen (Ref 2, 16):

$$O_2 + 2H_2O + 4e^{-} \rightarrow 4OH^{-} \quad \text{(Eq 3)}$$

For the composite with 0.48 vol.% alumina particles, first the potential dropped to ~−1250 mV, then up to 600 s progressively rose to ~−1000 mV and fluctuated in phase with the reciprocating motion of the alumina ball. Competition between the mechanical depassivation and electrochemical passivation rates causes the potentials to fluctuate as long as the sliding continues (Ref 17). For the composite strip with 1.13 vol.% reinforcement, at first the OCP dropped to ~−1250 mV. Then up to 750 s the potential increased to ~−1050. Finally, for the composite sample with 3.55 vol.% Al_2O_3 particles, first the potential dropped to ~−1250 mV, then up to 600 s rose to ~−1000 mV. In general, it can be stated that the OCP variations of all the three composite strips and even the fluctuations of the OCP during rubbing are very similar. After stopping the rubbing, the OCP first rapidly rose and then progressively returned to a steady state value. In fact, after wear test, due to the occurrence of the repassivation of aluminum matrix the OCP increases abruptly and a positive shift in potentials is observed. The most increase of the repassivation potential takes place for the composite sample with 0.48 vol.% alumina. In general, from the discussed results it can be concluded that the depassivation and repassivation processes occur, respectively, at the beginning and the end of sliding wear test. This depassivation-repassivation process is almost similar for various composite strips.

The optical microscopy images of the wear track for composites with 0.48, 1.13, and 3.55 vol.% Al_2O_3 particles are shown in Fig. 5. The composite strip with 0.48 vol.% alumina

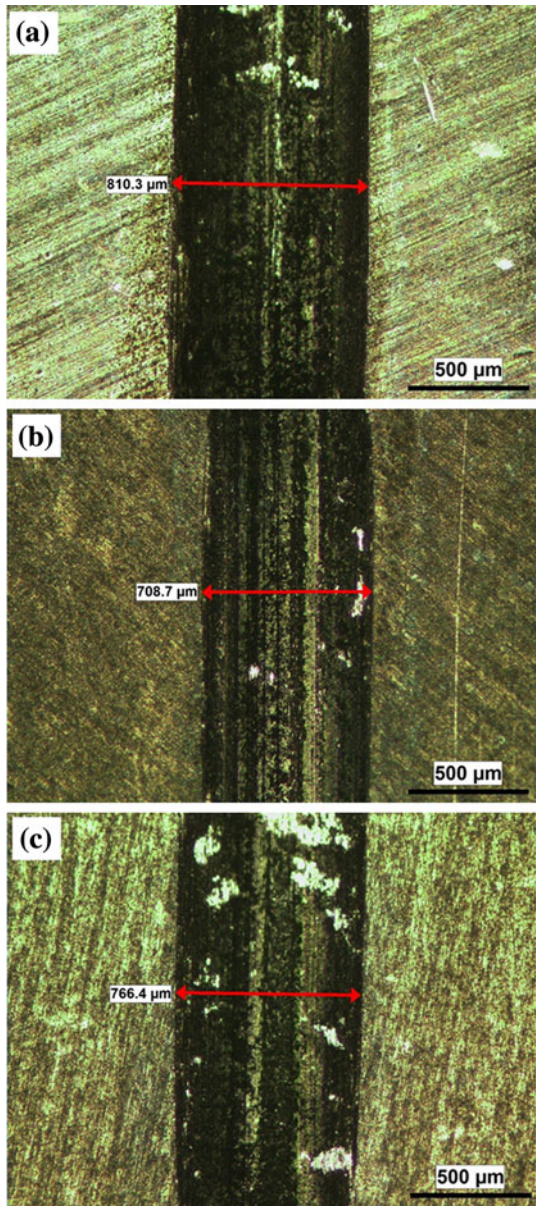

Fig. 5 OM images of the wear tracks after 1800 cycles of sliding on ARBed composites with (a) 0.48, (b) 1.13, and (c) 3.55 vol.% Al_2O_3

was most affected by the test, and the wear track width was largest compared to other samples. Furthermore, for the composite with 1.13 vol.% reinforcement, the width of wear track was smallest. In fact, Al/1.13 vol.% alumina had the highest wear resistance. It has been reported that the wear resistance of particle-reinforced composites is influenced by many factors such as (a) size of particles, (b) shape of particles, (c) nature and hardness of particles, (d) volume fraction of particles, (e) distribution of particles, (f) properties of matrix alloy, (g) bonding quality between particles and matrix, (h) applied load, and (i) sliding distance and speed. In our research, the factors such as (c), (f), (g), and (h) were constant for all three composite samples. However, the size, shape, volume fraction, and distribution of reinforcement particles (alumina) changed. It has been stated (Ref 4, 18, 19) that finer size, spheroid shape, higher volume fraction, and better distribution

of particles improve the wear resistance. The difference between composites with 0.48 and 1.13 vol.% alumina originates in size and volume fraction of particles. Although the composite with 0.48 vol.% Al_2O_3 has finer size, the volume fraction of particles for the composite with 1.13 vol.% alumina is higher. From wear track results, it can be concluded that for two later samples, the effect of volume fraction is more important compared to the particle size effect. The difference between composites with 1.13 and 3.55 vol.% alumina is related to size, shape, volume fraction, and distribution of particles. Although, the volume fraction of Al/3.55 vol.% alumina is higher, the conditions of other factors are better for the composite with 1.13 vol.% Al_2O_3. In other words, for Al/1.13 vol.% alumina, the size of particles is finer, the shape of alumina is spheroid, and the distribution of particles in the matrix is more uniform. Therefore, it can be argued that three later factors in Al/1.13 vol.% alumina overcome the higher volume fraction effect of the composite with 3.55 vol.% reinforcement.

It has been reported (Ref 20) that the tribocorrosion behavior of AISI 316 tested in aggressive environments consisted of two processes. First, in the wear track, the mechanical delamination of the passive layer occurred, and then, a progressive electrochemical repassivation of that active wear track area took place (indicating that because of the mechanical wear a part of the wear track lost its passive character). In general, metals such as stainless steel and aluminum are passive materials. These metals are protected from corrosion by a dense and passive oxide film. The part of the passive film can be damaged or removed as a result of sliding contact of the two surfaces.

3.3 EIS Results

The Bode plots of the coatings after 1 h of immersion in 1 wt.% NaCl solution before running the sliding test are presented in Fig. 6. The value of impedance $|Z|$ is plotted as a function of the phase shift Arg (Z). It is clear that the Arg (Z) plot of all composite strips is shifted toward high angles at medium frequencies (~1.5 Hz) indicating the passive film formation in 1 wt.% NaCl solution and a more capacitive response of the film. In contrast, this is down to zero at high frequencies. Meanwhile, the values of impedance for all the three ARBed composite strips are similar.

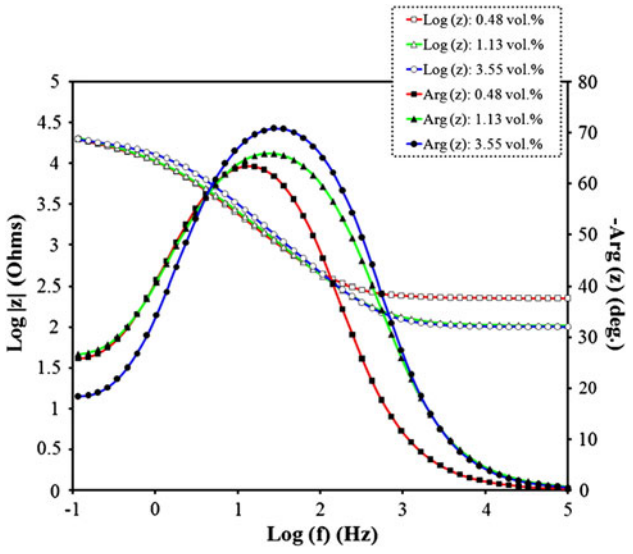

Fig. 6 Bode diagrams of eight cycle ARBed composites with 0.48, 1.13, and 3.55 vol.% alumina after 1 h immersion in 1 wt.% NaCl solution before running the sliding test

The spectra of all composite samples are characterized by a one time-constant behavior, and thus can be simulated by Randle circuit as a basic equivalent circuit presented in Fig. 7. In fact, the Randle circuit can be used for representing the corrosion characteristics of the samples because one peak is observed in the Arg (Z) plot. Such a circuit consists of the following features: (a) R_s corresponds to the solution resistance of the test electrolyte between the working electrode and the reference electrode, (b) C_{dl} or Q_{dl} is the double-layer capacitance which represents the charge build-up at the interface between the sample surface and the electrolyte, (c) R_{ct} is the charge transfer resistance, and (d) W is the Warburg impedance.

As the corrosion process at an electrochemical interface is complicated, EIS simulation often requires the use of complex circuit elements such as the constant phase element, Q, which is used to replace the capacitor C. This impedance is expressed as (Ref 2, 21):

$$Z_Q = [Y_0(jw)^n]^{-1}, \quad \text{(Eq 4)}$$

where Z_Q is the impedance (Ω cm^2), Y_0 is the parameter of Q (Ω^{-1} s^n cm^{-2} or F s^{n-1} cm^{-2}), and w is the angular frequency (rad/s). The parameter n is a constant, which shows the degree of deviation from ideal capacitive behavior that always lies between -1 and 1. Depending on the value of exponent n, the physical meaning of Q can be attributed to pure capacitor ($n = 1$), pure resistor ($n = 0$), and pure inductance ($n = -1$).

The experimental EIS spectra of all the three composite samples using the abovementioned Randle circuit were simulated and the best-fit curves are shown in Fig. 6. The data extracted from the AC impedance spectra by simulation, using the equivalent circuit described in Fig. 7 is shown in Table 1. For the ARBed composite with 0.48 vol.% alumina particles, R_{ct} was found to be 15.71 kΩ cm^2. The value of n was close to unity (0.8837). For composite strip with 1.13 vol.% Al_2O_3 particles,

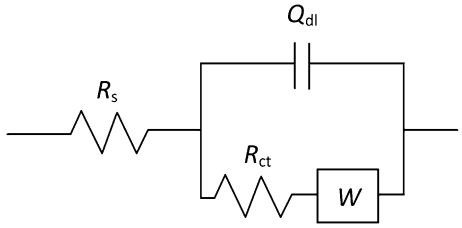

Fig. 7 Randle circuit used to simulate the EIS spectra

Table 1 Characteristics of the equivalent circuits derived from the simulation of EIS spectra

Sample, vol.%	R_s, Ω cm^2	Q_{dl} (Y_0), F/cm^2	Q_{dl}, n	R_{ct}, kΩ cm^2	W
0.48	100	7.76×10^{-6}	0.8837	15.71	1.87×10^{-4}
1.13	104	1.20×10^{-5}	0.8298	14.97	1.18×10^{-4}
3.55	225	1.22×10^{-5}	0.8499	14.44	1.29×10^{-4}

R_{ct} was 14.97 kΩ cm^2 while it was 14.44 kΩ cm^2 for aluminum/3.55 vol.% alumina composite strip. The n values of two later ARBed composites were 0.8298 and 0.8499, respectively. As can be seen, all these values are close to unity, too. Therefore, Al/0.48 vol.% Al_2O_3 composite sample has the highest charge transfer resistance while the strip with 3.55 vol.% alumina has the lowest R_{ct}. This means that the composite including 0.48 vol.% Al_2O_3 has the highest and aluminum/3.55 vol.% alumina composite the lowest corrosion resistance. The lowest corrosion resistance of Al/3.55 vol.% Al_2O_3 composite sample is attributed to the presence of more aluminum/alumina interface areas (which are much more suitable places for corrosion in MMCs) and also the lowest homogeneous distribution of alumina particles in the aluminum matrix.

Since the surface area before the sliding wear test was homogeneous, normalizing the EIS results for the surface area was possible. The exposed surface after the sliding wear test included the worn area that was inside the wear track and nonworn area that was outside the wear track. Therefore, it is impossible to normalize the EIS results for the entire surface area (Ref 2). For the ARBed composite with 0.48 vol.% alumina particles, R_{ct} was 8.87 kΩ cm^2 compared to 15.71 kΩ cm^2 before sliding. This difference indicates that the passive film formed in the active area of the wear track, 20 min after the end of sliding, has not yet regained its protective properties.

As can be concluded from the obtained results in this work, the composite including 0.48 and 1.13 vol.% alumina particle manufactured by anodizing and eight ARB cycles are promising for the applications in the automotive and aerospace industries because it has improved mechanical (Ref 12) and tribological properties. Mechanical properties of these composites were discussed in our previous article (Ref 12). Further studies, focused on corrosion, texture, TEM, and EBSD investigations are now in progress.

4. Conclusions

The tribocorrosion behavior of aluminum/alumina composites with various reinforcement quantities produced by anodizing and ARB processes was tested in the 1 wt.% NaCl solution. The OCP measurements were used to keep track of in situ degradation of the composite's surface in the NaCl solution. A drop in the OCP indicated the removal of the oxide film and the exposure of the active metal to the environment. The effect of the size, shape, quantity, and dispersion of alumina particles on tribocorrosion behavior was also evaluated. Uniformity distribution of Al_2O_3 particles in the Al matrix proved to improve the wear and corrosion resistance. In order to assess charge transfer resistance in the investigated composite strips the EIS method was used, which demonstrated that an increase in the alumina quantity correlates with lowering the value of R_{ct}.

References

1. L. Benea, F. Wenger, P. Ponthiaux, and J.P. Celis, Tribocorrosion Behaviour of Ni-SiC Nano-Structured Composite Coatings Obtained by Electrodeposition, *Wear*, 2009, **266**, p 398–405
2. M. Azzi, M. Paquette, J.A. Szpunar, J.E. Klemberg-Sapieha, and L. Martinu, Tribocorrosion Behaviour of DLC-Coated 316L Stainless Steel, *Wear*, 2009, **267**, p 860–866
3. T.M. Lillo, Enhancing Ductility of Al6061 + 10 wt.% B_4C Through Equal-Channel Angular Extrusion Processing, *Mater. Sci. Eng. A*, 2005, **410–411**, p 443–446
4. K.M. Shorowordi, T. Laoui, A.S.M.A. Haseeb, J.P. Celis, and L. Froyen, Microstructure and Interface Characteristics of B4C, SiC and Al_2O_3 Reinforced Al Matrix Composites: A Comparative Study, *J. Mater. Process. Technol.*, 2003, **142**, p 738–743
5. A. Upadhyaya and G.S. Upadhyaya, Sintering of Copper-Alumina Composites Through Blending and Mechanical Alloying Powder Metallurgy Routes, *Mater. Des.*, 1995, **16**, p 41–45
6. D.Y. Ying and D.L. Zhang, Processing of Cu-Al_2O_3 Metal Matrix Nanocomposite Materials by Using High-Energy Ball Milling, *Mater. Sci. Eng. A*, 2000, **226**, p 152–156
7. D.J. Lloyd, Particles Reinforced Aluminum and Magnesium Matrix Composites, *Int. Mater. Rev.*, 1994, **39**, p 1–23
8. H. Ferkel, Properties of Copper Reinforced by Laser-Generated Al_2O_3-Nanoparticles, *Nanostruct. Mater.*, 1999, **11**, p 595–602
9. R. Jamaati, M.R. Toroghinejad, and A. Najafizadeh, An Alternative Method of Processing MMCs by CAR Process, *Mater. Sci. Eng. A*, 2010, **527**, p 2720–2724
10. R. Jamaati, M.R. Toroghinejad, and A. Najafizadeh, Application of Anodizing and CAR Processes for Manufacturing Al/Al_2O_3 Composite, *Mater. Sci. Eng. A*, 2010, **527**, p 3857–3863
11. R. Jamaati and M.R. Toroghinejad, Manufacturing of High-Strength Aluminum/Alumina Composite by Accumulative Roll Bonding, *Mater. Sci. Eng. A*, 2010, **527**, p 4146–4151
12. R. Jamaati and M.R. Toroghinejad, High-Strength and Highly-Uniform Composite Produced by Anodizing and Accumulative Roll Bonding Processes, *Mater. Des*., 2010, **31**(10), p 4816–4822
13. R. Jamaati and M.R. Toroghinejad, Effect of Al_2O_3 Nano-Particles on the Bond Strength in CRB Process, *Mater. Sci. Eng. A*, 2010, **527**, p 4858–4863
14. F. Bratu, L. Benea, and J.P. Celis, Tribocorrosion Behaviour of Ni-SiC Composite Coatings Under Lubricated Conditions, *Surf. Coat. Technol.*, 2007, **201**, p 6940–6946
15. M. Azzi and J.A. Szpunar, Tribo-Electrochemical Technique for Studying Tribocorrosion Behavior of Biomaterials, *Biomol. Eng.*, 2007, **24**, p 443–446
16. E.E. Stansbury and R.A. Buchanan, *Fundamentals of Electrochemical Corrosion*, ASM International, Materials Park, OH, 2000
17. P. Ponthiaux, F. Wenger, D. Drees, and J.P. Celis, Electrochemical Techniques for Studying Tribocorrosion Processes, *Wear*, 2004, **256**, p 459–468
18. C.Y.H. Lim, S.C. Lim, and M. Gupta, Wear Behaviour of SiC_p-Reinforced Magnesium Matrix Composites, *Wear*, 2003, **255**, p 629–637
19. M. Kok and K. Ozdin, Wear Resistance of Aluminium Alloy and Its Composites Reinforced by Al_2O_3 Particles, *J. Mater. Process. Technol.*, 2007, **183**, p 301–309
20. I. Garcia, D. Drees, and J.P. Celis, Corrosion-Wear of Passivating Materials in Sliding Contacts Based on a Concept of Active Wear Track Area, *Wear*, 2001, **249**, p 452–460
21. Sh. Hassani, K. Raeissi, M. Azzi, D. Li, M.A. Golozar, and J.A. Szpunar, Improving the Corrosion and Tribocorrosion Resistance of Ni-Co Nanocrystalline Coatings in NaOH Solution, *Corros. Sci.*, 2009, **51**, p 2371–2379